J. Electroanal. Chem., 142 (1982) 67–84
Elsevier Sequoia S.A., Lausanne – Printed in The Netherlands

THE OXYGEN EVOLUTION ON $La_{0.5}Ba_{0.5}CoO_3$

OVERPOTENTIAL DECAY BEHAVIOUR: THEORY AND EXPERIMENTAL RESULTS

A.G.C. KOBUSSEN *, H. WILLEMS and G.H.J. BROERS

Department of Inorganic Chemistry, State University of Utrecht, Croesestraat 77A, 3522 AD Utrecht (The Netherlands)

(Received 22nd December 1981; in revised form 28th May 1982)

ABSTRACT

In section (I) the overpotential decay behaviour of an electrode during oxygen evolution is described on the basis of calculations for two mechanisms with a chemical rate-determining step (rds). Quasi-equilibrium in the steps preceding the rds and Frumkin-type adsorption of intermediates is assumed. In section (II) decay experiments are reported for oxygen evolution on $La_{0.5}Ba_{0.5}CoO_3$ in 6 *M* KOH solution at room temperature. Both aged and renewed oxide electrodes were used. Measured decay rates at constant overpotential were found to vary as a function of starting overpotential, while the theory requires equal rates. Also, an increased capacitance for the aged electrode with respect to the renewed one was not accompanied by an expected increase in current density. Neither phenomenon can be explained by assuming non-equilibrium in the mechanism, but can be understood on the basis of a growing passive multilayer with a presumably enhanced Co^{IV}/Co^{III}-ratio. The peroxide mechanism with a chemical rds and low coverage of the second intermediate is the most likely of the alternatives considered. Capacitances calculated from the initial overpotential decay were approximately equal to capacitances derived from ac impedances measured prior to the interruption.

(I) THEORETICAL DESCRIPTION OF THE OVERPOTENTIAL DECAY

(I.1) Introduction

Measurement of the (open-circuit) overpotential decay of an electrochemical cell after steady-state potentiostatic polarization was used to characterize the oxygen evolution process on $La_{0.5}Ba_{0.5}CoO_3$. This method was originally developed to study the discharge of an ionic double-layer capacitance [1], but was later also used for the characterization of oxygen evolution at nickel (oxide) electrodes [2] and of chlorine evolution [3]. The method can give kinetic information equivalent to that

* Present address: Materials Research Dept., VEG-Gasinstituut n.v., P.O. Box 137, 7300 AC Apeldoorn, The Netherlands.

0022-0728/82/0000–0000/$02.75

derived from Tafel plots in steady-state measurements, but additionally can give information about the electrode capacitance. The occurrence of a pseudo-capacitance resulting from adsorbed intermediates complicates the analysis of decay measurements but this problem was previously handled for the hydrogen evolution reaction by numerically exploring applicable mechanisms [3,4].

Conway [2] stated that measurement of the overpotential decay has the added advantage of giving well-defined data on an electrode that is subject to (partial) oxidation. In that case, steady-state experiments would not give meaningful results over the entire overpotential range. This was indeed established earlier in the steady-state polarization study on $La_{0.5}Ba_{0.5}CoO_3$ [5]. Decay measurements should then give results that are entirely controlled by the state of the electrode at the time of interruption. But it remains doubtful whether these decays can be easily interpreted, since the situation at the electrode after interruption changes almost as if a quasi-steady-state experiment with decreasing overpotential had been performed.

An obvious advantage of the current interruption method is that no ohmic resistances have to be corrected for. The apparatus needed can be kept simple if systems with large pseudo-capacitances and therefore large relaxation times are studied; in that case pen recorders will suffice.

The interpretation of overpotential decays for a constant electrode capacitance is straightforward [6]. From a plot of overpotential η vs. the logarithm of time t, the electrode capacitance C, Tafel slope b and exchange current density i_0 may be deduced according to

$$\eta = b\log(bC/2.3i_0) - b\log(t+\tau) \tag{1}$$

with $\tau = bC/2.3i_{\text{init}}$.

The overpotential–time relation can more generally be derived by considering not the time derivatives of capacitance and overpotential but rather the more elementary derivative $d(Q_{\text{surface}})/d\eta$ or $d\theta/d\eta$ as the relevant operator describing the decay process [3,4]. This approach will be applied to two mechanisms recently proposed for oxygen evolution at $La_{0.5}Ba_{0.5}CoO_3$ [5,7,8]. Numerically obtained characteristic plots will be shown, since in general no analytical solutions can be derived. In section (II) these results will be compared with experimental decays obtained after anodically polarizing a $La_{0.5}Ba_{0.5}CoO_3$ electrode. Finally, the validity of the mechanisms and the usefulness of the method will be discussed.

(I.2) Derivation of the theoretical model

The mechanisms to be discussed are the Krasil'shchikov mechanism and the peroxide mechanism involving two intermediates [7,8]. In the following scheme both are shown:

Peroxide mechanism	Krasil'shchikov mechanism
1. $OH^- \rightleftharpoons OH_{ad} + e$	1. $OH^- \rightleftharpoons OH_{ad} + e$
2. $OH_{ad} + OH^- \rightleftharpoons O_{ad} + H_2O + e$	2a. $OH_{ad} + OH^- \rightarrow O_{ad}^- + H_2O$ (rds)
3. $O_{ad} + OH^- \rightarrow O_2H_{ad}^-$ (rds)	

Steps following the rate-determining step (rds) are not taken into consideration, since they are assumed to have no influence on the course of the reaction. This is certainly justified under quasi-equilibrium conditions, i.e. steps (1) and (2) are essentially in equilibrium, and provided no accumulation of other intermediates than $OH_{ad}(\theta_1)$ and $O_{ad}(\theta_2)$ takes place.

In the following derivations the symmetry coefficients will be taken equal to $\frac{1}{2}$ and the rate of the back reaction in the rds will be neglected. Furthermore, Frumkin-type adsorption will be adopted, with an overall interaction parameter g describing the interaction effect of the adsorbates via the total surface coverage, as discussed earlier [8]. The overpotential decay for the Krasil'shchikov mechanism can be derived from that of the more complex peroxide mechanism, so the latter will be treated first.

The total current density i_t in the system consists of a contribution by the (faradaic) electrochemical process, i_F, and a double-layer charging current, viz. *.

$$i_t = i_F + q_{dl}(dH/dt) \tag{2}$$

The current density i_F is found by application of material balances for both θ_1 and θ_2 (see ref. 8 for a complete derivation) which leads to the following expression in i_s (steady-state current density) and $q\, d\theta/dt$:

$$i_F = i_s + \sum q\frac{d\theta}{dt} = 4L_3\theta_2 \exp(\tfrac{1}{2}g\theta_t) + 2q_1\frac{d\theta_1}{dt} + 4q_2\frac{d\theta_2}{dt} \tag{3}$$

During an overpotential decay the total (external) current is zero, so

$$i_s = 4L_3\theta_t\left(\frac{\theta_2}{\theta_t}\right)\exp(\tfrac{1}{2}g\theta_t) = -\left(2q_1\frac{d\theta_1}{d\theta_t} + 4q_2\frac{d\theta_2}{d\theta_t} + q_{dl}\frac{dH}{d\theta_t}\right)\frac{d\theta_t}{dt} \tag{4}$$

where all variables are given in terms of the total surface coverage θ_t by the introduction of conversion factors.

Another way of expressing eqn. (4) shows the decay rate to be dependent on both overpotential and surface coverages

$$-\frac{dH}{dt} = \frac{i_s}{q_{dl} + 2q_1\dfrac{d\theta_1}{dH} + 4q_2\dfrac{d\theta_2}{dH}} \tag{5}$$

with i_s defined in eqn. (4). As will be shown below (eqn. 9), the various surface coverages are unique functions (albeit transcendental) of the overpotential alone, provided the preceding electrochemical steps are in quasi-equilibrium. This unique dependence of dH/dt on H also holds for other mechanisms under quasi-equilibrium conditions of the steps preceding the rds. An important result of this quasi-equilibrium approach is the equality of decay rates $-dH/dt$ for constant value of H, irrespective of the starting potential H_0. Thus, a set of experimentally

* See the list of symbols at the end of the text.

measured decay curves starting from different η_0 values should yield a set of equal $-d\eta/dt$ values at various constant overpotentials.

An alternative representation of the decay process makes use of logarithmic decay slopes $d\eta/d\log t$. The relation with the previously introduced decay slopes is

$$-\frac{d\eta}{dt} = -\frac{t}{2.3}\frac{d\eta}{d\log t} \tag{6}$$

A simple increase in the surface roughness factor of the electrode alone should have no effect upon the validity of eqn. (5), since i_s, q_1, q_2 and q_{dl} are all proportional to this roughness factor. Furthermore, it can be proven that all H (or η) vs. $\log t$ curves tend to coincide when $H_0 - H > 4.6$, i.e. $\eta_0 - \eta > 110$ mV (at ambient temperature). Therefore, when different decay rates at equal overpotentials are found there is some kind of non-stationary behaviour acting, for example a lagging surface coverage [9] and/or a slow depassivation effect.

In addition, it follows from the basic eqns. (2) and (3) that

$$-\left(\frac{d\eta}{dt}\right)_{t\to 0} = \frac{i_{s0}}{C_{dl}(\eta_0) + C_p(\eta_0)} = \frac{i_{s0}}{C(\eta_0)} \tag{7}$$

where i_{s0} is the stationary current just before interruption and $C(\eta_0)$ the total capacitance at the (iR_Ω-corrected) steady-state overpotential η_0. Since C_{dl} will not vary strongly with η, any serious variation of the experimentally observable $C(\eta_0)$ should reflect a change of the pseudo-capacitance C_p and the associated θ's with the overpotential. However, it should again be stressed that all equations are based upon the assumption of an "infinite" exchange current (quasi-equilibrium) of the electrochemical steps (1) and (2) in the mechanism. For very short decay times (corresponding to very high frequencies in impedance measurements), this assumption may not hold [8]. Then the analysis becomes very complex, in particular when the influence of C_{dl} is taken into account. Whereas in the case of ac impedance the relevant equations can at least be linearized [8], this is no longer allowed in the present case where substantial potential changes are involved. Moreover, reliable measurements of $(d\eta/dt)_{t\to 0}$ are difficult to perform when the "time constant" involved $\Delta\eta C(\eta_0)/i_{s0} < 5$–$10$ μs ($\Delta\eta \ll RT/F$). As with high-frequency impedance measurements, these problems arise mainly from inductive (ringing) effects (enhanced here by the large dc current to be interrupted).

To evaluate the precise form of the decay curves for the peroxide mechanism, eqn. (4) can be integrated which leads to

$$-4L_3\int_{t_0}^{t} dt = \int_{\theta_0}^{\theta} \frac{q_{dl}\frac{dH}{dt} + 2q_1\frac{d\theta_1}{d\theta_t} + 4q_2\frac{d\theta_2}{d\theta_t}}{\left(\frac{\theta_2}{\theta_t}\right)\theta_t \exp\left(\frac{1}{2}g\theta_t\right)} d\theta_t \tag{8}$$

From the kinetic equations for the various steps the conversion factors $d\theta_1/d\theta_t$, $d\theta_2/d\theta_t$, $dH/d\theta_t$ and θ_2/θ_t can be derived (see Appendix 1) and are found to be

functions of both θ_t and H. Under quasi-equilibrium conditions of steps (1) and (2) the θ_t, H relation has been derived earlier [8]

$$\theta_t(1-\theta_t)^{-1}\exp g\theta_t = K_I(1+K_{II}) = P_I \exp H(1+P_{II}\exp H) \tag{9}$$

Since eqn. (9) is transcendental these conversion factors cannot be given solely in θ_t, and thus eqn. (8) cannot be evaluated analytically. Note that K_I and K_{II} incorporate overpotential terms according to, for example, $K_I = P_I \exp H$. The notation used is fully explained in our earlier publication on the impedance behaviour of this mechanism [8].

Before treating eqn. (8) numerically, a useful simplification can be made by assuming Langmuir-type adsorption ($g = 0$). With assumed equal maximal surface charges q_1 and q_2, this leads to the following integral:

$$-4L_3 t = q_{dl}\int_{H_0}^{H} \frac{1+K_I+K_IK_{II}}{K_IK_{II}}\,dH + 2q\int_{H_0}^{H} \frac{1+4K_{II}+K_IK_{II}}{K_{II}(1+K_I+K_IK_{II})}\,dH \tag{10}$$

which is derived and then solved analytically in Appendix 2. The evaluation of this equation is dependent only on the choice of equilibrium constants P_I and P_{II} and will be shown below, together with the results of the numerical approach for three sets of P_I, P_{II} values, considered earlier in the theoretical evaluation of the impedance response of the peroxide mechanism [8].

(I.3) Numerical results

The complete integral of eqn. 8 for $q_1 = q_2 = q$ has been calculated by a numerical integration routine for a number of equilibrium constants and parameters g. For each value of H then, before evaluating the expression under the integral sign, the associated value of θ_t is found by solving eqn. (9) numerically as described earlier [8]. Together with the time t the derivatives $dH/d\ln t$, $dH/d\ln i$, $d\theta_1/dH$ and $d\theta_2/dH$, and from the latter two the pseudo-capacitance C_p are also calculated.

Results for a number of dimensionless starting overpotentials H_0 are shown in figs. 1 and 2 as a function of H and g for the first case considered, i.e. $P_I = 10^{-3}$ and $P_{II} = 10^{-5}$. The plots of H vs. $\log t$ (Fig. 1) and of the decay slope $dH/d\ln t$ vs. H (Fig. 2) are suitable for comparison with experimental results. Another useful experimental representation is to plot $\log(-d\eta/dt)$ vs. η, as will be shown in section (II). As noted above (section I.2), corresponding plots of $\log(-dH/dt)$ vs. H obtained from various starting potentials H_0 should yield coinciding curves on the basis of the present theory. Thus, any deviation from the latter is directly noticed in this type of plot.

As was clearly derived by Conway [10], the decay slope $-dH/d\ln t$ should be numerically larger than the (differential) Tafel slope $dH/d\ln i$ for increasing capacitance with overpotential, and vice versa for falling capacitances past the capacitance maximum. This simple rule, i.e. crossing of the $-dH/d\ln t$ and $dH/d\ln i$ curves at a capacitance maximum, is seen to hold only for the second (at a higher overpotential) of the two capacitance maxima. The pseudo-capacitance and surface coverage

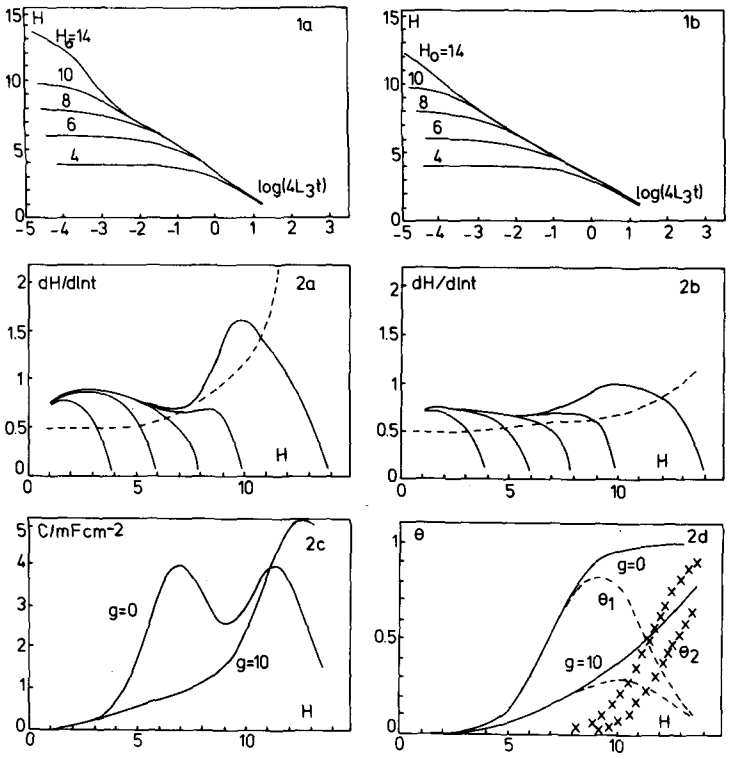

Fig. 1. Numerically obtained overpotential decay curves starting from different overpotentials H_0 for the peroxide mechanism with $P_I = 10^{-3}$, $P_{II} = 10^{-5}$, $q = 2 \times 10^{-4}$ C cm^{-2}, $q_{dl} = 8 \times 10^{-7}$ C cm^{-2}; (a) for $g = 0$ and (b) for $g = 10$.

Fig. 2. (a) Dimensionless decay slopes for the curves of Fig. 1a. Dashed lines signify dimensionless Tafel slopes ($dH/d \ln i$); (b) as (a) for the curves of Fig. 1b; (c) capacitance curve based on $q = 2 \times 10^{-4}$ C cm^{-2}; (d) associated surface coverages: (———) total coverage; (— — —) θ_1; (× × ×) θ_2.

behaviour, although published earlier [8], are also shown in Fig. 2 for clarity. In this and following theoretical calculations q was taken to be 2×10^{-4} C cm^{-2} ★ and q_{dl} as 8×10^{-7} C cm^{-2} (based on a constant double-layer capacitance of ≈ 30 μF cm^{-2}). By calculating some curves for other values of q_{dl} it was found that they are far more sensitive to changes in P_I and P_{II} than in the q/q_{dl} ratio. However, as will be shown in the two cases considered below, the maximum in the logarithmic decay rate at high overpotentials is governed by the value of q_{dl}.

★ Careful calculation of q based on the assumption of one active site per unit cell in $La_{0.5}Ba_{0.5}CoO_3$ leads to a value of $q = 10^{-4}$ C cm^{-2}, but in view of the relative insensitivity of the curves to the q/q_{dl} ratio the earlier assumed value (2×10^{-4} C cm^{-2}) was maintained.

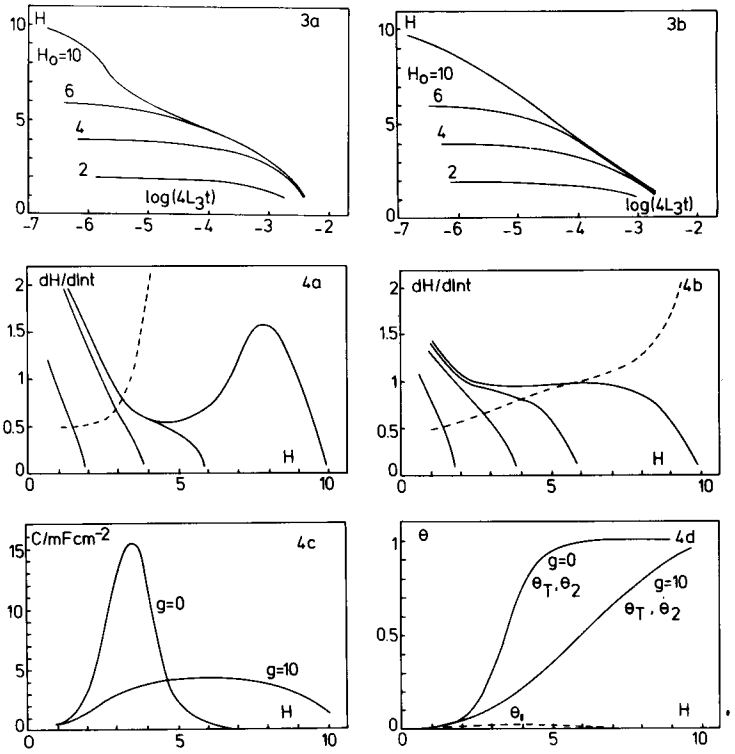

Fig. 3. Numerically obtained overpotential decay curves starting from different overpotentials H_0 for the peroxide mechanism with $P_I = 10^{-3}$, $P_{II} = 1$, $q = 2 \times 10^{-4}$ C cm^{-2}, $q_{dl} = 8 \times 10^{-7}$ C cm^{-2}; (a) for $g = 0$ and (b) for $g = 10$.

Fig. 4. (a) Dimensionless decay slopes for the curves of Fig. 3a. Dashed lines signify dimensionless Tafel slopes ($dH/d \ln i$); (b) as (a) for the curves of Fig. 3b; (c) capacitance curve; (d) associated surface coverages: (———) total coverage ($= \theta_2$); (— — —) θ_1.

The second case is shown in Figs. 3 and 4, corresponding to $P_I = 10^{-3}$ and $P_{II} = 1$. Under these conditions ($P_I \ll P_{II}$) the second intermediate O_{ad} *is made to dominate* the surface coverage. Now the mechanism behaves almost like the Krasil'shchikov mechanism with its second (chemical) step rate determining. As previously shown, in that case the Tafel slope found (Fig. 4a and 4b) has to be multiplied by two to obtain the real Tafel slope for the Krasil'shchikov mechanism. The same holds for the decay slope and again the numerically obtained results can be checked for $g = 0$, since then an analytical expression analogous to the transcendental one of eqn. (9) can be derived for the simpler Krasil'shchikov mechanism.

Finally, a third case is considered in Figs. 5 and 6 by choosing $P_I = 10^{-1}$ and $P_{II} = 10^{-10}$. In this case ($P_I \gg P_{II}$), only substantial surface coverage of the first

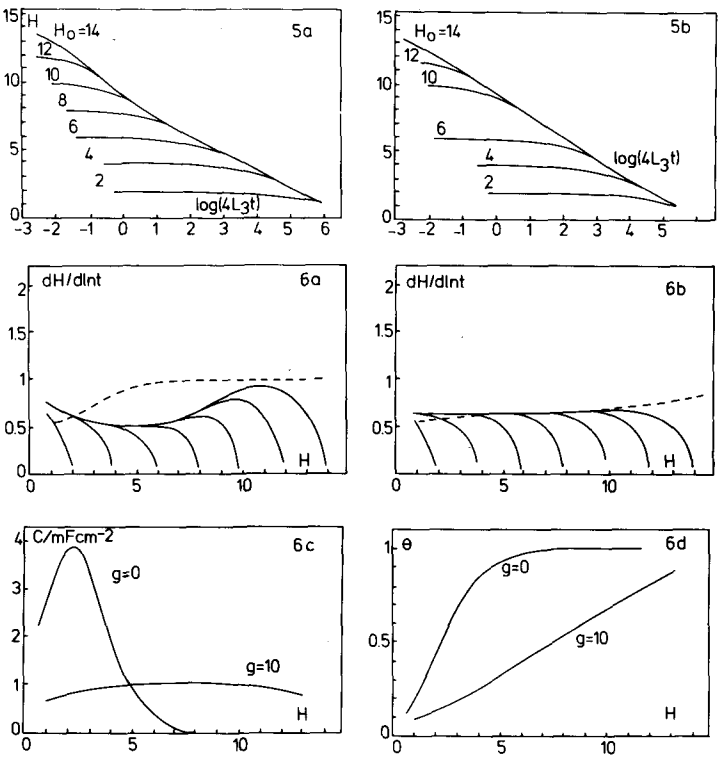

Fig. 5. Numerically obtained overpotential decay curves starting from different overpotentials H_0 for the peroxide mechanism with $P_I = 10^{-1}$, $P_{II} = 10^{-10}$, $q = 2 \times 10^{-4}$ C cm^{-2}, $q_{dl} = 8 \times 10^{-7}$ C cm^{-2}; (a) for $g = 0$ and (b) for $g = 10$.

Fig. 6. (a) Dimensionless decay slopes for the curves of Fig. 5a. Dashed lines signify dimensionless Tafel slopes ($dH/d \ln i$); (b) as (a) for the curves of Fig. 5b; (c) capacitance curve; (d) associated surface coverage ($= \theta_1$, θ_2 being negligibly small).

intermediate (OH_{ad}) is found, whereas θ_2 stays very low. This choice of constants is interesting, since pseudo-capacitances caused by θ_1 are independent of the kinetic behaviour that is primarily controlled by θ_2 [8]. It is seen from Fig. 6 that the Tafel slope and decay slope cross as expected at the capacitance maximum. Here, as for the cases considered earlier, for $g = 0$ (Fig. 6c) the contribution of C_{dl} to the decay curves predominates only for $H > 9$; below $H = 7$ only the pseudo-capacitance C_p contributes. For $g = 10$ the entire decay curve is independent of C_{dl}.

(II) EXPERIMENTAL OVERPOTENTIAL DECAYS

(II.1) Experimental

The $La_{0.5}Ba_{0.5}CoO_3$ used and the electrochemical equipment is the same as described earlier [5,7]. The circular electrode had a diameter of 5.2 mm and was rotated at an angular velocity of 188 rad s^{-1}. The electrolyte used was 6 *M* potassium hydroxide kept at room temperature. The current was interrupted manually with a mercury switch. Decay potentials were first buffered with a variable gain adjustable offset differential amplifier and then recorded on a pen recorder. Ohmic resistance drops and overpotential decays below 2 s were measured via the buffer amplifier with a transient recorder in pre-trigger mode and later plotted on an X–Y pen recorder. All potentials were measured with respect to a Hg/HgO electrode in the same solution, but all overpotentials are given with respect to the reversible oxygen electrode in the same solution. All current densities stated were calculated on the basis of geometrical surface areas.

(II.2) Results and discussion

A sequence of decay experiments with successively lower starting potentials was performed beginning at $\eta_0 = 401$ mV. After each decay (duration 1–1.5 h) the overpotential was set at a lower η_0 value and the dc current allowed to stabilize. This took typically 16 h at high overpotentials down to 4 h at about 250 mV. Results for an aged electrode are shown in Figs. 7–9. Previously it had been subjected to a large number of slow anodic potential sweeps (total charge passed estimated at 2.5×10^5 C cm^{-2} geometrical area). After this series the electrode surface was renewed by grinding, polishing and cleaning, and then subjected to a similar series of decay experiments, typical results of which are shown in Fig. 10. Starting overpotentials η_0 (corrected for *iR* drop) are given in Table 1, along with current densities *i*, capacitance values $C(\eta_0) = -i(\mathrm{d}\eta/\mathrm{d}t)^{-1}_{t\to 0}$ (cf. eqn. 7), and *iR* corrections, all at the moment of current interruption.

Figures 7 and 8 for the aged electrode can be compared with the various theoretical *H* vs. $\log t$ and $\mathrm{d}H/\mathrm{d}\ln t$ vs. *H* plots respectively, shown in section (I) (Figs. 1–6). From the three cases considered, the last one ($P_{\mathrm{I}} = 10^{-1}$, $P_{\mathrm{II}} = 10^{-10}$), illustrated by Figs. 5 and 6, is seen to give the best fit, provided an intermediate interaction parameter *g* between 0 and 10 is chosen. However, the experimental $\log(-\mathrm{d}\eta/\mathrm{d}t)$ vs. η curves plotted in Fig. 9 show convincingly that $-\mathrm{d}\eta/\mathrm{d}t$ is by no means constant at constant η. As discussed in section (I), this constancy should hold when the preceding electrochemical steps are in quasi-equilibrium.

Figure 9 shows that the decay rates at constant η increase quite systematically with decreasing starting potential η_0. A similar trend is found for the renewed electrode in Fig. 10 (but with one significant exception: the first curve starting at 433 mV shows larger decay rates than the second one starting at 424 mV; see the discussion below). The initial capacitances $C(\eta_0)$ all increase modestly with decreas-

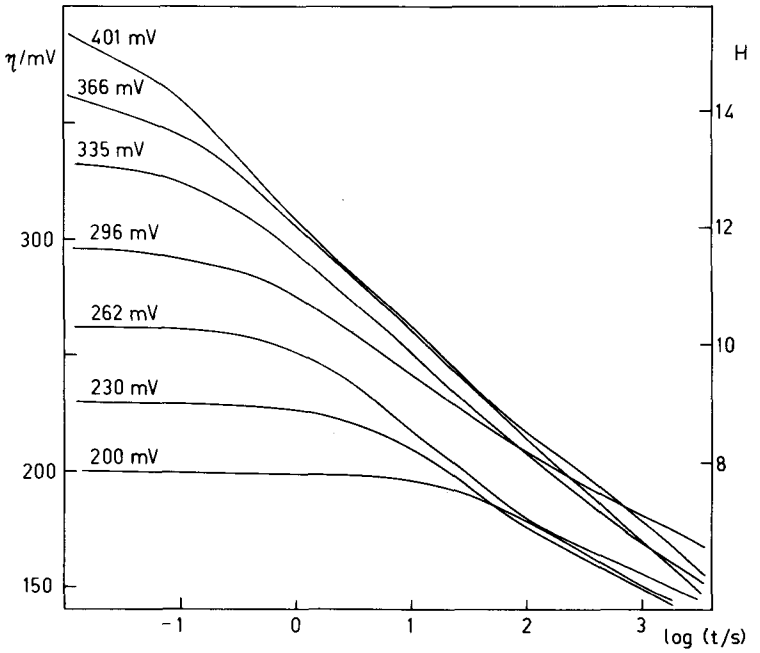

Fig. 7. Overpotential decay vs. $\log t$ curves for an aged electrode in 6 M KOH. Starting overpotentials (η_0) from high to low in chronological order.

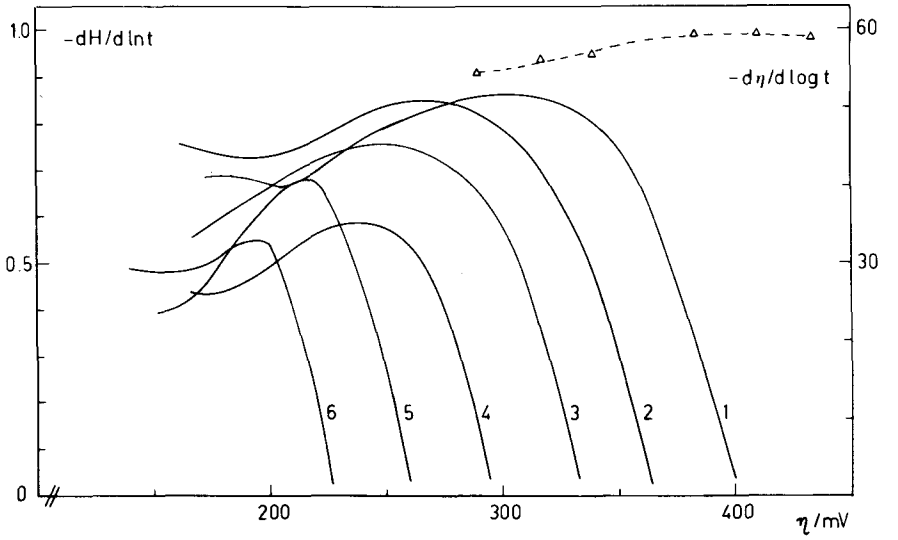

Fig. 8. $-\mathrm{d}\eta/\mathrm{d}\log t$ vs. η curves corresponding to Fig. 7, in chronological order. (△) Differential Tafel slopes ($\mathrm{d}\eta/\mathrm{d}\log i$) obtained from combined dc and ac admittance experiments [7] for another but similarly aged electrode.

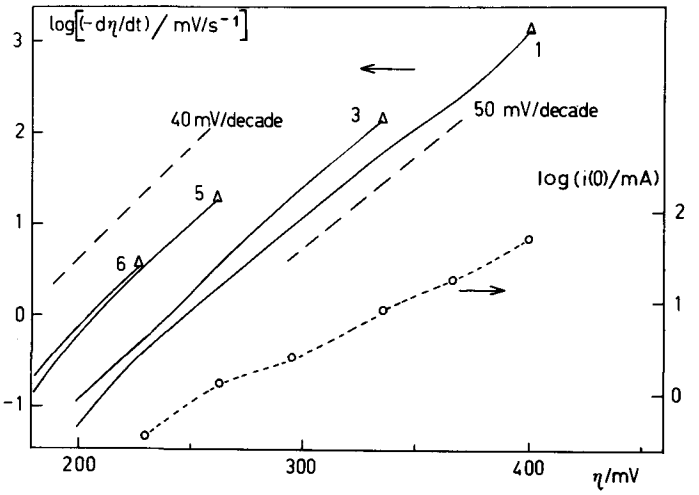

Fig. 9. Log($-d\eta/dt$) vs. η curves for the aged electrode, cf. Figs. 7 and 8. (△) Starting overpotential (η_0). Also shown are log i ($t=0$) values (○) just before current interruption at various η_0. These curves point to increasing passivation effects caused by prolonged polarization at increasingly higher overpotentials (for clarity, not all curves are shown).

ing η_0 (cf. Table 1), but for the aged electrode these are 3.4–4.4 times larger than those for the renewed specimen. This difference may in part be caused by the greater surface roughness of the aged electrode. However, an increased surface roughness

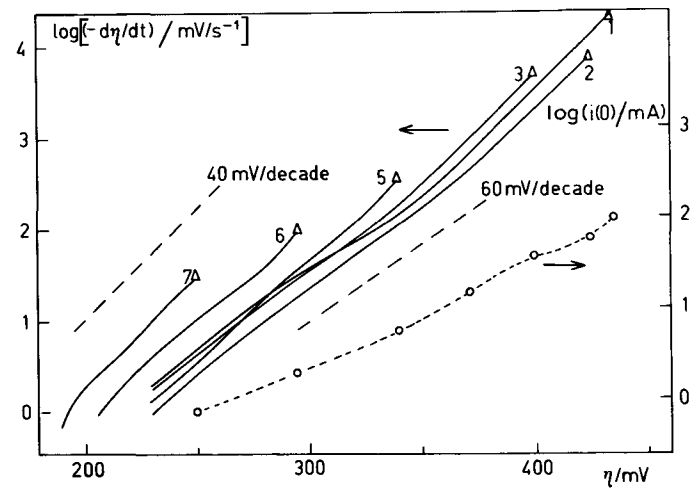

Fig. 10. Log($-d\eta/dt$) vs. η curves for the renewed electrode and corresponding log i ($t=0$) (○). Note the lower position of curve 2 compared to curve 1 as discussed in the text (for clarity, not all curves are shown).

TABLE 1

Starting overpotentials η_0 (in chronological order) and current densities i, initial capacitances $C(\eta_0)$ and iR corrections measured at the moment of interruption

Aged electrode				Renewed electrode			
η_0/mV	i/mA cm^{-2}	C/mF cm^{-2}	iR/mV	η_0/mV	i/mA cm^{-2}	C/mF cm^{-2}	iR/mV
401	250.0	179	107.0	433	463.0	22.0	217.0
366	83.8	245	34.0	424	277.0	35.5	127.0
335	38.4	298	14.8	399	171.0	41	75.7
296	11.9	310	5.2	369	68.0	70	29.3
262	6.0	309	2.4	339	25.4	75	10.9
230	1.6	423	–	296	9.1	91	4.0
(200)	(0.3)			249	3.3	117	1.3

alone would lead to a corresponding increase in steady-state current density, and this is clearly not the case, as shown by Table 2 (derived from data of Table 1).

Moreover, as noted above, the first two experiments on the renewed electrode show a similar discrepancy between the steady-state currents and corresponding capacitances. A current ratio $i(2)/i(1) = 1.06$ is predicted on the basis of the observed ratio $C(2)/C(1) = 35.5/22.0$ and accounting for the difference in overpotential (424 mV vs. 433 mV); the observed ratio is 0.60.

These phenomena cannot be interpreted on the basis of the relatively simple model involving two adsorbed intermediates with assumed monolayer coverages. Even when the assumption of quasi-equilibrium in steps (1) and (2) is abandoned (leading to very complicated mathematics), no large discrepancies between the aged and renewed electrode should be expected [9,11]. A more plausible assumption is the formation on the $La_{0.5}Ba_{0.5}CoO_3$ substrate at high overpotentials of a (partially) passive multilayer with a higher Co^{IV}/Co^{III} ratio than is present in the substrate proper, where this ratio is equal to unity. This multilayer could be the predominant contributor to the effective electrode capacitance. As long as the available Co^{III} sites

TABLE 2

Comparison of current and initial capacitance ratios for aged and renewed electrodes at almost identical overpotentials

Approx. η_0/mV	$i_{aged}/i_{renewed}$	$C(\eta_0)_{aged}/C(\eta_0)_{renewed}$
400	1.46	4.37
368	1.23	3.50
337	1.51	3.97
296	1.30	3.41

supposed to be necessary for the oxygen evolution reaction (OER) are scarce, the decay rates will be relatively small. When after each decay to very low overpotentials the electrode is again polarized to successively lower starting overpotentials, the multilayer will not be restored to its previous extent (and the electrode capacitance may either increase or decrease). But in any case more Co^{III} sites can be expected and thus the OER and corresponding decay rates at equal overpotential will be enhanced in a relative sense.

For the aged electrode, the passivation effect seems to become unimportant at starting overpotentials below about 250 mV, since Fig. 9 reveals nearly coinciding curves for the two lowest η values. In addition, relatively fast (4 h) stabilization of the current at these low starting overpotentials occurs. The behaviour of the renewed electrode (Fig. 10) is less regular, probably due to continuing surface-roughening effects in the course of the time-consuming experiments.

On the basis of the present data it is not possible to give a detailed description of the OER mechanism. Nevertheless, some interesting points can be noted:

(1) When a simple anodic Tafel relation is adopted for the rds in the OER mechanism, which after current interruption proceeds through discharge of a capacitance $C(\eta)$, the potential decay rate is given by the elementary equation

$$-\frac{d\eta}{dt}=\frac{i(\eta)}{C(\eta)}=\frac{i_o \exp\frac{2.3\eta}{b}}{C(\eta)} \tag{11}$$

or

$$\log\left(-\frac{d\eta}{dt}\right)=\log i_0-\log C(\eta)+\frac{\eta}{b} \tag{12}$$

where $i(\eta)$ is an internal (not measurable) current corresponding to the OER. The type of representation used in eqn. (12) is demonstrated in Figs. 9 and 10. If $C(\eta)$ were constant, linear plots would be observed in these figures with (reciprocal) slopes equal to the Tafel slope b. In Fig. 9, b is seen to vary between 50 and 40 mV/decade over an overpotential range down to about 200 mV. Taking into account the modest increase of $C(\eta_0)$ with decreasing η_0, most of the increase of the intercept $\log i_0/C(\eta)$ must be caused by an increase in effective i_0 upon lower prepolarization.

Finally, the curvature of the various plots in Fig. 9 is in part due to the changing $C(\eta)$ and would be less pronounced if $C(\eta)$ were constant. So the Tafel slopes and thus the kinetics of the rds are essentially unaltered over the potential region considered.

(2) It should be noted that the Tafel slopes apparent from Fig. 9 may also be deduced from the $-d\eta/d\log t$ vs. η curves of Fig. 8 (which represent eqn. (1), the integrated form of eqn. 11), but only so where $\eta_0-\eta>2b$. In our opinion the representation of Fig. 9 is more informative than that of Fig. 8, though the data are basically the same.

(3) The build-up of a multilayer with a higher Co^{IV}/Co^{III} ratio on a similarly

renewed $La_{0.5}Ba_{0.5}CoO_3$ electrode at overpotentials below 250–300 mV was also shown from combined dc and ac (impedance) measurements reported previously [7]. A relatively large "parasitical" dc current and a (most probably) related "parasitical" ac admittance were observed when the renewed electrode was slowly polarized from 150 mV up to ≈ 280 mV (for details, see ref. 7). At higher overpotentials and also for an aged electrode, the parasitical ac contribution was no longer detectable, and there the admittance could simply be interpreted in terms of a parallel combination of a non-ideal (cpa type) capacitance C_{eff} and a faradaic admittance Y_F. Trends for C_{eff} to increase modestly with decreasing η down to about 200 mV, were qualitatively similar to those observed for $C(\eta_0)$ in the present decay experiments.

(4) However, for the aged electrode used in the ac experiments [7] (total charge passed 8×10^4 C cm^{-2}) C_{eff} ranged from 22 to 43 mF cm^{-2}, whereas $C(\eta_0)$ for the present more aged electrode (total charge 2.5×10^5 C cm^{-2}) ranges from 179 to 423 mF cm^{-2} over the same potential range. This raises the question whether $C(\eta_0)$ as found from initial decay rates should be equal to C_{eff} found from small ac perturbation techniques. If the latter can be performed in a relatively short time (approx. 5 min for a frequency range 10 kHz–0.1 Hz) preceding the current interruption, one may indeed expect roughly equal C values. This will of course only be so when on the one hand the ac equivalent circuit can be represented by a simple parallel RC combination, and on the other hand $(-d\eta/dt)_{t\to 0}$ upon interruption is constant over an initial potential decrease $\ll RT/F$ (5 mV say). Checks of this kind impose heavy demands on the electronic equipment used to monitor the initial decay rate (in connection with ringing effects below 0.1 ms), but preliminary tests on another aged electrode have shown that $C(\eta_0)$ and C_{eff} remain equal within a factor of 2. These results suggest that a combination of ac and current interruption methods with advanced equipment can yield very useful information where both fast and slow adsorption/desorption phenomena are involved in electrode processes.

(5) On the basis of electrochemical evidence alone, the nature of the multilayer cannot be identified. In its ultimate form this may alternatively be a chemically different top layer or a structurally unchanged layer of basic material with modified electrocatalytic or conductive properties. Post-test analyses of the electrode interfaces, substantiating a slight chemical alteration of the surface layer will be discussed in a further communication [12].

(II.3) Conclusions

The overpotential decay experiments on "aged" and "renewed" $La_{0.5}B_{0.5}CoO_3$ electrodes do not show the equal decay rates $d\eta/dt$ at equal potentials that are predicted by the theory presented here based upon quasi-equilibrium conditions for the electrochemical steps preceding a supposed chemical rds in the OER. Only at low overpotentials (< 200 mV) and for sufficiently "aged" electrode surfaces (exposed to vigorous O_2 evolution over extended periods) could the theoretical model be applicable, in the sense that quasi-equilibrium conditions are approached and adsorbed intermediates (OH_{ads}, O_{ads}) may be present in monolayer form. At higher

overpotentials a distinct (partial) passivation phenomenon effectively reduces the number of electroactive sites on which the rds in the OER proceeds. Most probably the passivation is caused by the formation of Co^{IV}-rich (hydrated) oxide multilayers. Increasingly higher overpotentials clearly enhance the stability of the passive layer. These phenomena are reflected in apparently increasing Tafel slopes for (pseudo) steady-state currents and depressed log[decay rates] curves for increasing starting overpotentials (Fig. 9). In view of the relatively small change in slope of the latter curves about 250 mV, the kinetics of the rds in terms of differential Tafel slopes (≈ 50 mV/decade) is not seriously affected by the passivation phenomenon, in contrast to its apparent i_0 value.

Because of the substantial surface-roughening effects during continued oxygen evolution, it is not possible to obtain information about the nature of the passivation layer from numerical capacitance values at various starting potentials. The mere fact that they are very large evidently causes the overall decay process to be very slow, which effect is still enhanced by the sparse availability of active sites for the rds (i.e. small i_0).

In section (I) the rds was assumed to be of a chemical rather than an electrochemical nature, based upon the previously observed first-order dependence of i ($\eta =$ const) upon a (OH^-) [5] in stationary experiments. However, these experiments had to be carried out on aged electrodes for obvious reasons and were necessarily restricted to the overpotential range 250–280 mV, where in view of the present results passivation (in 6 *M* KOH) becomes evident and the differential Tafel slope is ≈ 50 mV/ decade. The above-mentioned first-order dependence would require a slope of ≈ 60 mV/decade, as discussed previously [5,7]. Taking into account the uncertainty of the data, this points to the chemical nature of the rds. An unambiguous determination of reaction order with respect to the hydroxyl ion activity would require a more thorough (and probably difficult) investigation.

ACKNOWLEDGEMENT

We wish to thank H.J.A. van Wees for the numerous preliminary overpotential decays measured.

LIST OF SYMBOLS

b	Tafel slope $= 2.3 \propto F/RT$ (mV/decade)
C	capacitance (F cm^{-2})
F	Faraday's constant (C mol^{-1})
g	dimensionless interaction parameter in Frumkin-type adsorption, $= r/RT$
i	current density (A m^{-2})
i_0	exchange current density (A m^{-2})
i_{s0}, i_s	faradaic current density (A m^{-2})
K_I, K_{II}	potential-dependent equilibrium constants
L_3	equivalent electrochemical rate constant for a chemical step (A m^{-2})

P_I, P_{II}	equilibrium constants independent of overpotential
q	maximal surface charge (C m^{-2})
q_{dl}	maximal surface charge due to the ionic double layer (C m^{-2})
Q	surface charge (C m^{-2}); quantity defined in Appendix 2
R	gas constant
T	absolute temperature (K)
t	time (s)
Y	admittance (Ω^{-1} m^{-2})
α	electrochemical charge-transfer coefficient
H	dimensionless overpotential, $H = \eta F/RT$
η	overpotential (V)
θ	fractional surface coverage
τ	characteristic decay time constant given by eqn. (1)

APPENDIX 1

Derivation of the conversion factors in eqn. (8)

The convection factors are derived under quasi-equilibrium conditions of steps (1) and (2) starting from the following stationary relations:
for step (1)

$$\theta_1(1-\theta_t)^{-1}\exp(g\theta_t) = K_I = P_I \exp H \tag{A1.1}$$

for step (2)

$$\theta_2/\theta_1 = K_{II} = P_{II}\exp H \tag{A1.2}$$

where the meaning of the equilibrium constants P is discussed in an earlier publication [8]. From the latter expression it follows that

$$\theta_2 = \theta_1 K_{II} = (\theta_t - \theta_2)K_{II} \tag{A1.3}$$

and thus

$$\theta_2 = \theta_t K_{II}/(1+K_{II}) \tag{A1.4}$$

and

$$\theta_1 = \theta_2/K_{II} = \theta_t(1+K_{II})^{-1} \tag{A1.5}$$

Now the derivatives $d\theta_1/d\theta_t$ and $d\theta_2/d\theta_t$ are readily evaluated

$$\frac{d\theta_1}{d\theta_t} = \frac{1}{1+K_{II}} - \theta_t \frac{dH}{d\theta_t}\frac{K_{II}}{(1+K_{II})^2} \tag{A1.6}$$

$$\frac{d\theta_2}{d\theta_t} = \frac{K_{II}}{1+K_{II}} + \theta_t \frac{dH}{d\theta_t}\frac{K_{II}}{(1+K_{II})^2} \tag{A1.7}$$

The derivative $dH/d\theta_t$ is calculated by taking the total differential of the

function of $F(\theta_t, H)$ (eqn. 9)

$$F(\theta_t, H) = \theta_t(1-\theta_t)^{-1}\exp(g\theta_t) - K_I(1+K_{II}) = 0 \tag{A1.8}$$

From

$$\left(\frac{\partial F}{\partial H}\right)_{\theta_t} dH + \left(\frac{\partial F}{\partial \theta_t}\right)_H d\theta_t = 0 \tag{A1.9}$$

it follows that

$$\frac{dH}{d\theta_t} = -\left(\frac{\partial F}{\partial \theta_t}\right)_H \Big/ \left(\frac{\partial F}{\partial H}\right)_{\theta_t} = \left[\frac{1}{\theta_t(1-\theta_t)} + g\right]\frac{K_I(1+K_{II})}{K_I(1+2K_{II})} \tag{A1.10}$$

Given the transcendental relation between θ_t and H no further simplification is possible.

APPENDIX 2

The decay integral for the Langmuir case

By simply taking $g = 0$ all conversion factors in eqn. (8) can be given as functions of H since now

$$\theta_t = K_I(1+K_{II})/[1+K_I(1+K_{II})] \tag{A2.1}$$

is an explicit relation between θ_t and H. The resulting eqn. (10) is broken up into two integrals A and B, which will be handled in succession.

Let us first consider part A.

$$A \equiv \frac{-4L_3 t_{dl}}{q_{dl}} = \int_{H_0}^{H} \frac{1+K_I+K_IK_{II}}{K_IK_{II}}\, dH \tag{A2.2}$$

The evaluation of this integral can easily be accomplished by substituting $dx = d\exp(-H)$ which leads to

$$A = -\int_{x_0}^{x} \frac{x^2+P_Ix+P_IP_{II}}{P_IP_{II}x}\, dx = \frac{x_0^2-x^2}{2P_IP_{II}} + \frac{x_0-x}{P_I} + \ln\frac{x_0}{x} \tag{A2.3}$$

with $x_0 = \exp(-H_0)$ (the initial condition). The second fragment is likewise reduced to

$$\begin{aligned} B \equiv \frac{-4L_3 t_q}{2q} &= -\int_{x_0}^{x} \frac{x^2+4P_{II}x+P_IP_{II}}{P_{II}(x^2+P_Ix+P_IP_{II})}\, dx \\ &= \frac{1}{P_{II}}\left[x_0 - x + \frac{P_I-4P_{II}}{2}\ln\frac{x^2+P_Ix+P_IP_{II}}{x_0^2+P_Ix_0+P_IP_{II}}\right. \\ &\quad \left. -\tfrac{1}{2}Q\ln\frac{(2x+P_I-Q)(2x_0+P_I+Q)}{(2x+P_I+Q)(2x_0+P_I-Q)}\right] \end{aligned} \tag{A2.4}$$

with $Q = \sqrt{P_I(P_I - 4P_{II})}$ supposed to be real. When $P_I - 4P_{II} < 0$ the last term of B between brackets is given by

$$+Q'\left\{\tan^{-1}\left(\frac{2x + P_I}{Q'}\right) - \tan^{-1}\left(\frac{2x_0 + P_I}{Q'}\right)\right\} \tag{A2.5}$$

where $Q' = \sqrt{P_I(4P_{II} - P_I)}$.

REFERENCES

1 J.A.V. Butler and G. Armstrong, Trans. Faraday Soc., 29 (1933) 1261.
2 B.E. Conway and P.L. Bourgault, Trans. Faraday Soc., 58 (1962) 593.
3 B.V. Tilak and B.E. Conway, Electrochim. Acta, 21 (1976) 745.
4 B.V. Tilak, C.G. Radler and B.E. Conway, Electrochim. Acta, 22 (1977) 1167.
5 A.G.C. Kobussen and C.M.A.M. Mesters, J. Electroanal. Chem., 115 (1980) 131.
6 H.B. Morley and F.E.W. Wetmore, Can. J. Chem., 34 (1956) 359.
7 A.G.C. Kobussen, J. Electroanal. Chem., 126 (1981) 199.
8 A.G.C. Kobussen and G.H.J. Broers, J. Electroanal. Chem., 126 (1981) 221.
9 B.E. Conway, M.A. Sattar and D. Gilroy, Electrochim. Acta, 14 (1969) 711.
10 B.E. Conway, Theory and Principles of Electrode Processes, Ronald Press, New York, 1965, p. 157.
11 M.A. Sattar and B.E. Conway, Electrochim. Acta, 14 (1969) 695.
12 A.G.C. Kobussen, H. Willems and G.H.J. Broers, J. Electroanal. Chem., 142 (1982) 85.